IPC

Indonesian Physics Communication

Department of Physics, Universitas Riau, Pekanbaru, Indonesia
p-ISSN 1412-2960 | e-ISSN 2579-521X

Vol. 22 | No. 1
March 2025

Web: https://kfi.ejournal.unri.ac.id
E-mail: kfi@ejournal.unri.ac.id

Modification of magnetic properties and morphology of iron oxide particles of natural sand from Rokan River through copper doping and preparation using ball milling method

Elika Gultom, Salomo Sinuraya*, Erwin Amiruddin, Awitdrus
Department of Physics, Universitas Riau, Pekanbaru 28293, Indonesia

*Corresponding author: salomo@lecturer.unri.ac.id

ABSTRACT

The magnetic susceptibility, magnetic properties, morphological properties, and composition of iron oxide nanoparticles of the natural sand in Rokan River, Rokan Hulu Regency, doped copper and prepared by the ball milling method. Processing of the magnetic and non-magnetic particle separation was carried out using iron sand separator (ISS). The ball milling process is ground in two stages for 70 hours and 30 hours and is divided into 3 parts and doped copper with concentrations (weight%) 0 wt%, 5 wt%, and 10 wt%, called BM_{2A}, BM_{2B}, and BM_{2C} products. The calculation of the magnetic susceptibility of the sample is carried out based on the values (B_T) and (B_0). The resulting magnetic susceptibility decreases as the percentage of copper doping increases. Vibrating sample magnetometer (VSM) shows the magnetic properties of iron oxide particles produced, namely magnetization saturation (M_S) decreases, coercivity value (H_C) and loop squareness (M_r/M_S) grow up, and remanent magnetization (M_r) and loop area (A) varies as doping concentration increases. Morphological properties and composition of iron oxide particles using a scanning electron microscope with energy dispersive X-ray (SEM-EDX). The average measurement of particles produced decreased with the increase in copper doping given, that is 121.960 ± 47.493 nm, 119.730 ± 37.03 nm, and 84.244 ± 34.392 nm. Copper element increased with the increase in doping concentrations given which were 0.76%, 7.11%, and 8.13%, while elements O, Si, and Fe decreased.

Keywords: Ball milling; copper; iron oxide; natural sand; Rokan River

Received 01-05-2023 | Revised 18-12-2024 | Accepted 15-03-2025 | Published 31-03-2025

INTRODUCTION

One of the mining products that are widely discovered in Indonesia is iron sand. Iron sand is often found in coastal areas or rivers, particularly in Java, Sumatra, Sulawesi and Nusa Tenggara [1, 2].

The utilization of iron sand in Indonesia can be said to have not been processed optimally. So far, iron sand has only been used as a building material and is generally exported in raw form [3-5]. In fact, the existence of iron sand that is easy to find can make it easier to process and make it into a material that has a high selling value [1]. The mineral content in iron sand depends on its local source, namely magnetite (Fe_3O_4), hematite (α-Fe_2O_3), maghemite (γ-Fe_2O_3) [1, 6, 7]. Iron sand has very broad applications and can be said to be the center of attention for researchers, where it has applications in industry, electronics, computing, and household equipment [8-10].

The size of iron oxide particles can be reduced to a nanometer scale using the ball milling method. Ball milling is a tool or machine that is useful for managing materials made of metal and has characteristics that are hard, not easily broken and corrosion resistant [11, 12]. This ball milling process is a powder crushing process carried out by a collision mechanism between steel balls and samples in order to produce finer particles up to nanometer size. Factors that affect ball milling performance include rotation speed, tube shape, time, temperature, pressure, and powder weight composition [13-15].

Preparation of iron oxide nanoparticles from natural sand from the Rokan River was carried

out using the ball milling method. The characterization test of the vibrating sample magnetometer (VSM) and scanning electron microscope with energy dispersive X-ray (SEM-EDX) was carried out by providing copper (Cu) doping to the sample in order to see changes in the magnetic properties and morphology of iron oxide particles.

RESEARCH METHODS

Natural sand from Rokan River, Ujung Batu, Riau Province, Indonesia is the sample used in this study. The separation process between magnetic and non-magnetic particles was carried out with the help of an iron sand separator (ISS) tool, referred to as the B_{ISS} product. The B_{ISS} product was then milled in the first stage of ball milling for 70 hours by mixing 16 iron balls with a diameter of 2 cm with the sample into a tube at a speed of 100 rpm, referred to as the BM_1 product. The BM_1 product was then milled in the second stage of ball milling for 30 hours and doped with copper elements with concentrations (weight%) of 0 wt%, 5 wt% and 10 wt%, referred to as the BM_{2A}, BM_{2B}, and BM_{2C} products. The magnetic susceptibility values of the samples, BISS products, BM_1, BM_{2A}, BM_{2B}, and BM_2 were calculated and the changes in magnetic properties in the samples were determined using a VSM and the morphological properties and composition of the samples were determined using a SEM-EDX.

RESULTS AND DISCUSSION

Magnetic Induction Measurement Data of Coreless Solenoid (B_0)

Table 1 and the graph in Figure 1 show the magnetic induction measurement data of the coreless solenoid (B_0).

The graph in Figure 1 explains that the magnetic induction value produced increases with the increase in the electric current given. The lowest magnetic induction value at a current of 200 mA is 3.398 mT and the highest induction value at a current of 1000 mA is 11.626 mT.

Table 1. B_0 measurement results.

Current (mA)	B_0 (mT)
200	3.398
400	5.508
600	7.584
800	9.601
1000	11.626

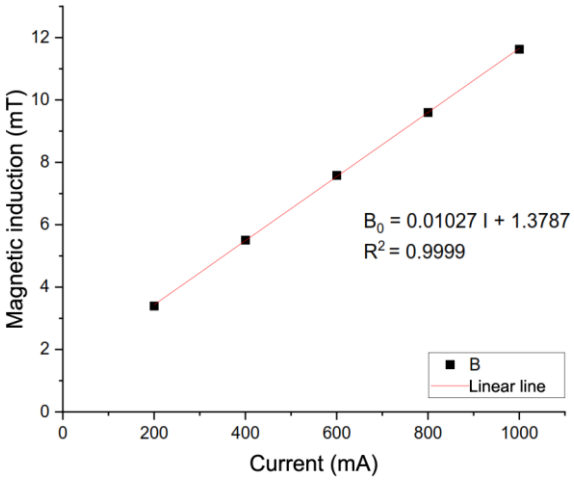

Figure 1. B_0 magnetic induction data graph.

Based on the linear equation obtained B_0 = 0.0103 I + 1.3787, R^2 = 0.9999, it shows that when the given current is eliminated I = 0 mA, the magnetic induction value produced is not immediately zero but B_0 is 1.3787 mT. This is due to the influence of the remaining energy and the earth's magnetic field on the solenoid. The R2 value has an interval of 0 – 1, when the value approaches 1, the resulting data is more accurate.

Solenoid Magnetic Induction Measurement Data with Natural Sand Sample Core (B_S)

Table 2 and the graph in Figure 2 show the solenoid magnetic induction measurement data with a natural sand sample core (B_S).

Table 2. B_S measurement results.

Current (mA)	B_0 (mT)
200	3.510
400	5.634
600	7.697
800	9.729
1000	11.931

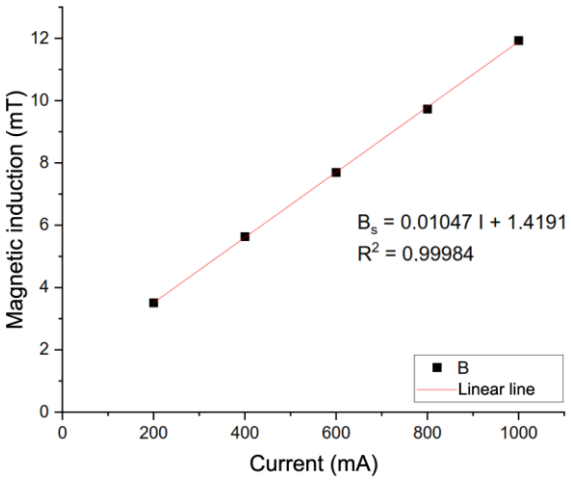

Figure 2. B_S magnetic induction data graph.

The graph in Figure 2 explains that the magnetic induction value produced increases with the increase in the electric current given. The lowest magnetic induction value at a current of 200 mA is 3.510 mT and the highest induction value at a current of 1000 mA is 11.931 mT.

Solenoid Magnetic Induction Measurement Data with ISS Product Sample Core (B_{ISS})

Table 3. B_{ISS} measurement results.

Current (mA)	B_0 (mT)
200	3.846
400	5.944
600	7.948
800	10.026
1000	12.204

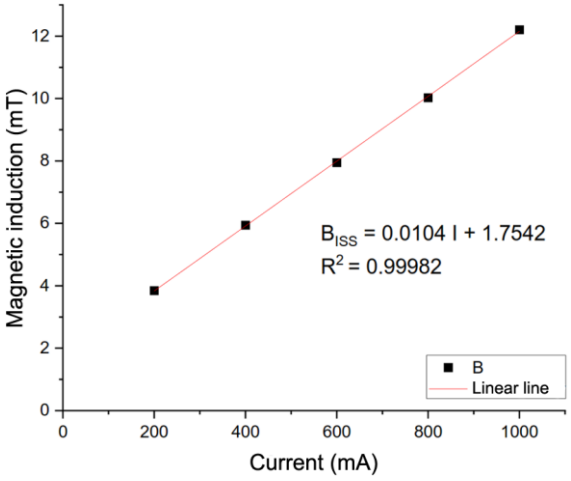

Figure 3. BISS magnetic induction data graph.

Table 3 and the graph in Figure 3 show the solenoid magnetic induction measurement data with an ISS product sample core (B_{ISS}). The graph in Figure 3 explains that the magnetic induction value produced increases with the increase in the electric current given. Based on Table 3. it can be seen that the magnetic induction value produced by the ISS product is greater than the magnetic induction value of the sample. This is because the ISS product has gone through a process of separating magnetic and non-magnetic particles, leaving more magnetic particles in it.

Solenoid Magnetic Induction Measurement Data with Multiple Product Sample Cores

The graphs in Figures 4, 5, 6, and 7 show the magnetic induction measurement data of the solenoid with the cores of the products BM_1, BM_{2A}, BM_{2B}, and BM_{2C}.

Figure 4 shows the graph of the magnetic induction value of the BM_1 product which is the first stage ball milling product for 70 hours using 16 iron balls with a diameter of 2 cm.

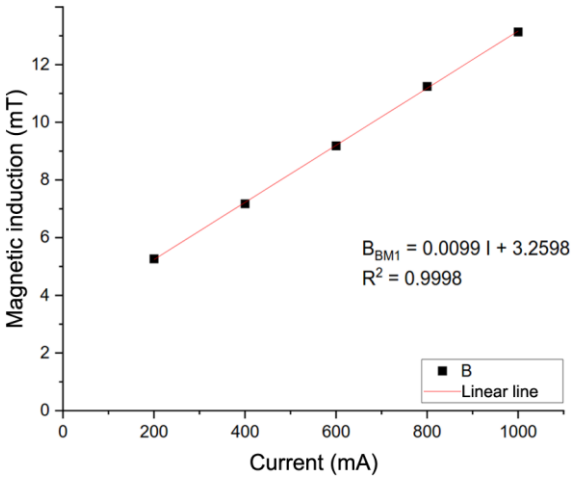

Figure 4. BM_1 magnetic induction data graph.

Figures 5, 6, and 7 show the magnetic induction graphs of the BM_{2A}, BM_{2B}, and BM_{2C} products which are the second stage ball milling products for 70 hours + 30 hours with 16 iron balls with a diameter of 2 cm and doped with copper elements with concentrations (weight%) of 0 wt%, 5 wt%, and 10 wt%. The magnetic induction values produced by the BM_{2A}, BM_{2B}, and BM_{2C} products are higher than the BM_1 product. This is due to the influence of the long

time of the ball milling process which results in a reduction in particle size that is getting smaller, thus increasing the number of iron oxide particles contained.

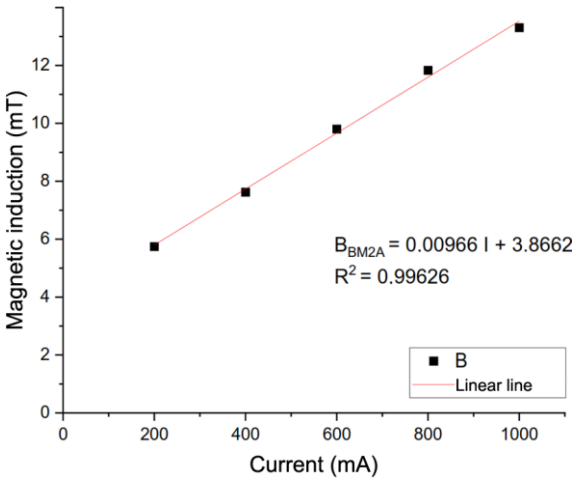

Figure 5. BM_{2A} magnetic induction data graph.

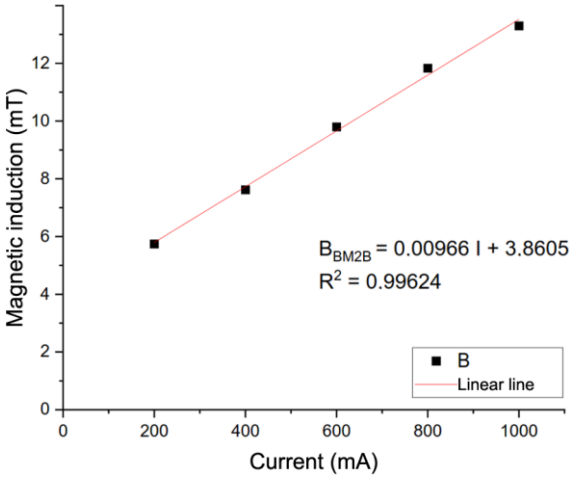

Figure 6. BM_{2B} magnetic induction data graph.

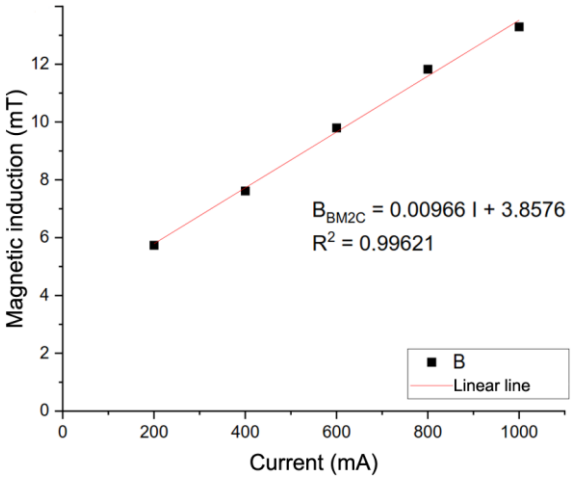

Figure 7. BM_{2C} magnetic induction data graph.

Magnetic Susceptibility Calculation Results (χ_m)

Table 4. Magnetic susceptibility data at a current of 1000 mA.

Sample	B_0 (mT)	B_T (mT)	χ_m (10^{-5})
Natural sand	11.626	11.931	2623.43
B_{ISS}	11.626	12.204	4791.61
BM_1	11.626	13.135	12979.52
BM_{2A}	11.626	13.305	14441.76
BM_{2B}	11.626	13.300	14398.76
BM_{2C}	11.626	13.296	14364.35

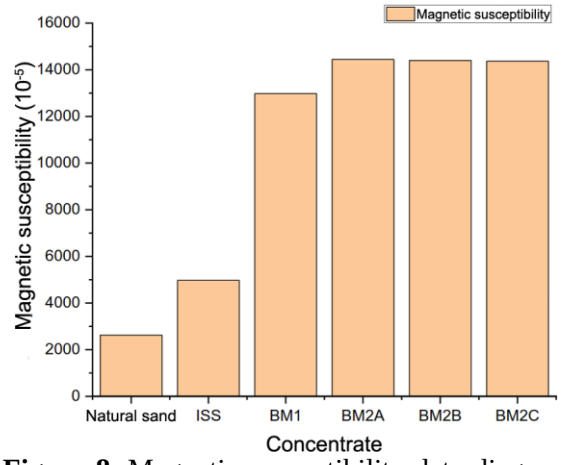

Figure 8. Magnetic susceptibility data diagram at a current of 1000 mA.

The results of the calculation of magnetic susceptibility data with a constant electric current of 1000 mA with a constant distance of 1 mm, on natural sand, ISS products, BM_1 products, BM_{2A} products, BM_{2B}, and BM_{2C} can be seen in Table 4 and the graph in Figure 8.

The data in Table 4. shows that the magnetic susceptibility value in natural sand samples has increased in the ISS product, this is because the ISS product has gone through a separation process between magnetic and non-magnetic particles so that more magnetic particles remain in it which causes the magnetic susceptibility value to be higher. The decrease in magnetic susceptibility value occurs in BM2A, BM2B, and BM2C products along with the increasing copper (Cu) doping given, because copper is a diamagnetic material that does not have a magnetic moment or its magnetism is weak, which causes the resulting susceptibility value to decrease along with increasing copper doping.

Scanning Electron Macroscope with Energy Dispersive X-Ray (SEM-EDX) Data

SEM characterization test was conducted to determine the changes in morphological properties found in BM_{2A}, BM_{2B}, and BM_{2C} products with a magnification of 5000 times as in Figure 9.

The SEM test results of BM2A, BM2B, BM2C products, namely the shape of the particles that vary and by using ImageJ software, the average size of the particles produced can be seen in Table 5. Basically, the shape of the hematite sample is or others. The results show that the magnetic nanoparticles produced are predominantly round, however, there are some magnetic nanoparticles produced that have irregular and asymmetric shapes. This is due to the ineffectiveness of destroying samples of the same size in ball milling process.

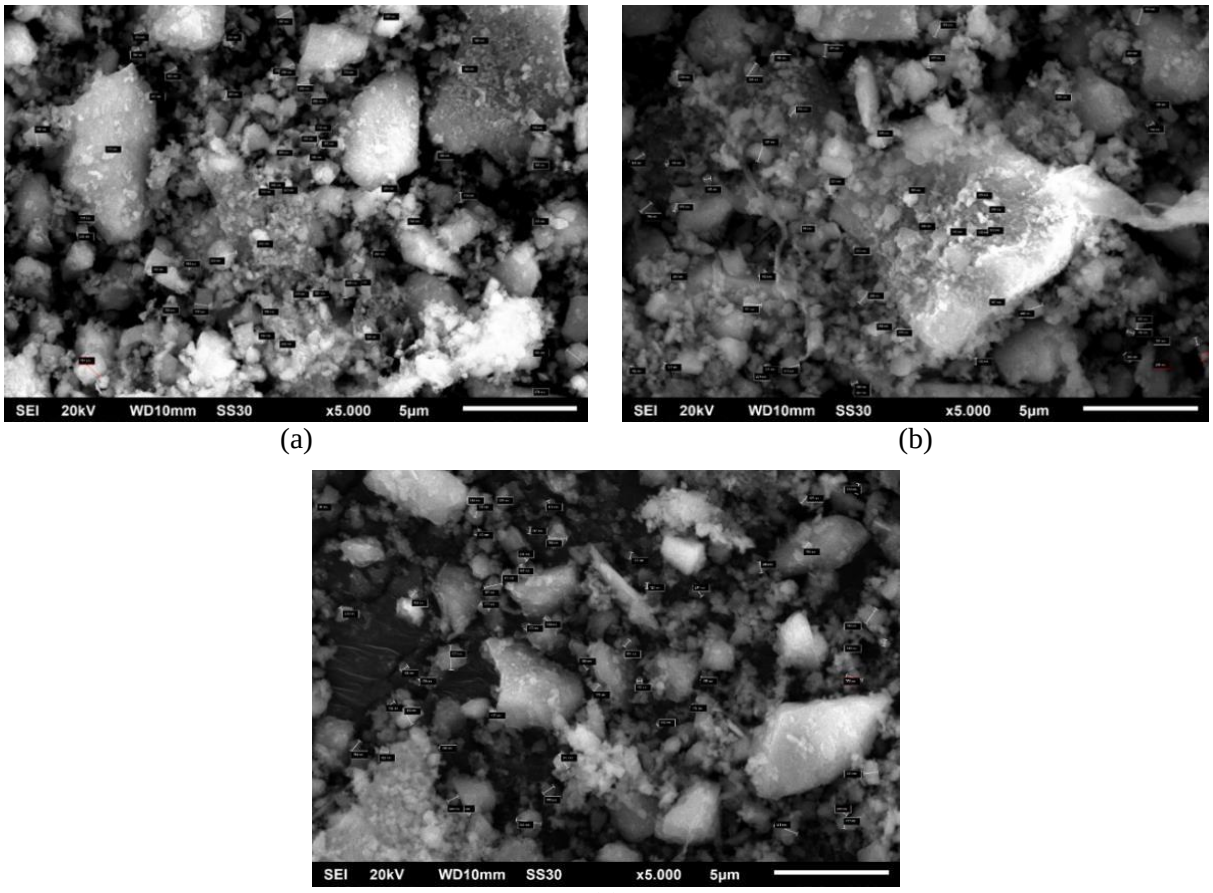

(a) (b)

(c)

Figure 9. Particle size of ball milling products at 5000 times magnification with copper doping (a) 0 wt%, (b) 5 wt%, and (c) 10 wt%.

Table 5. Average size of iron oxide particles.

Sample	Average size (nm)	Standard deviation
BM_{2A}	121.960	± 47.493
BM_{2B}	119.730	± 37.03
BM_{2C}	84.244	± 34.392

The EDX characterization test was carried out with the aim of determining changes in the elemental composition contained in the BM_{2A}, BM_{2B}, and BM_{2C} products as in Table 5.

The elements Fe and Si decreased as seen in Table 6. Along with the increase in copper doping given to BM_{2A}, BM_{2B}, and BM_{2C} products. This is because copper is a diamagnetic material that does not have a magnetic moment and its magnetism is weak, while Fe is a ferromagnetic that is strongly attracted by a magnet causing Fe to decrease, due to the influence of copper. Si decreased due to the influence of the length of the ball milling

process carried out which caused Si, which is a non-magnetic particle, to be removed from it.

Vibrating Sample Magnetometer Data

The results of the VSM characterization test were carried out to determine changes in the magnetic properties of the BM2A, BM2B, and BM2C products as shown in Figure 10 and Table 7.

The resulting magnetic properties are decreasing saturation magnetization (M_S), remanent magnetization (M_r) with a wide loop (A) that varies with increasing doping given to the BM_{2A}, BM_{2B}, and BM_{2C} products. Coercivity (H_c) and Loop squareness (M_r/M_S) increased.

Table 6. Elemental content in BM_{2A}, BM_{2B}, and BM_{2C} products.

Element	Mass (%)		
	BM_{2A}	BM_{2B}	BM_{2C}
C	17.52	18.40	47.6
O	23.88	18.98	13.03
Na	1.43	1.71	0.78
Mg	1.02	1.16	0.51
Al	5.26	5.48	2.36
Si	25.32	22.78	7.87
K	0.99	2.20	0.44
Ca	1.22	1.45	0.66
Ti	0.38	0.40	0.18
Fe	22.22	19.08	18.01
Cu	0.76	7.11	8.13
Zr	0.00	1.25	0.00
Zn	0.00	0.00	0.43
Total	100.00	100.00	100.00

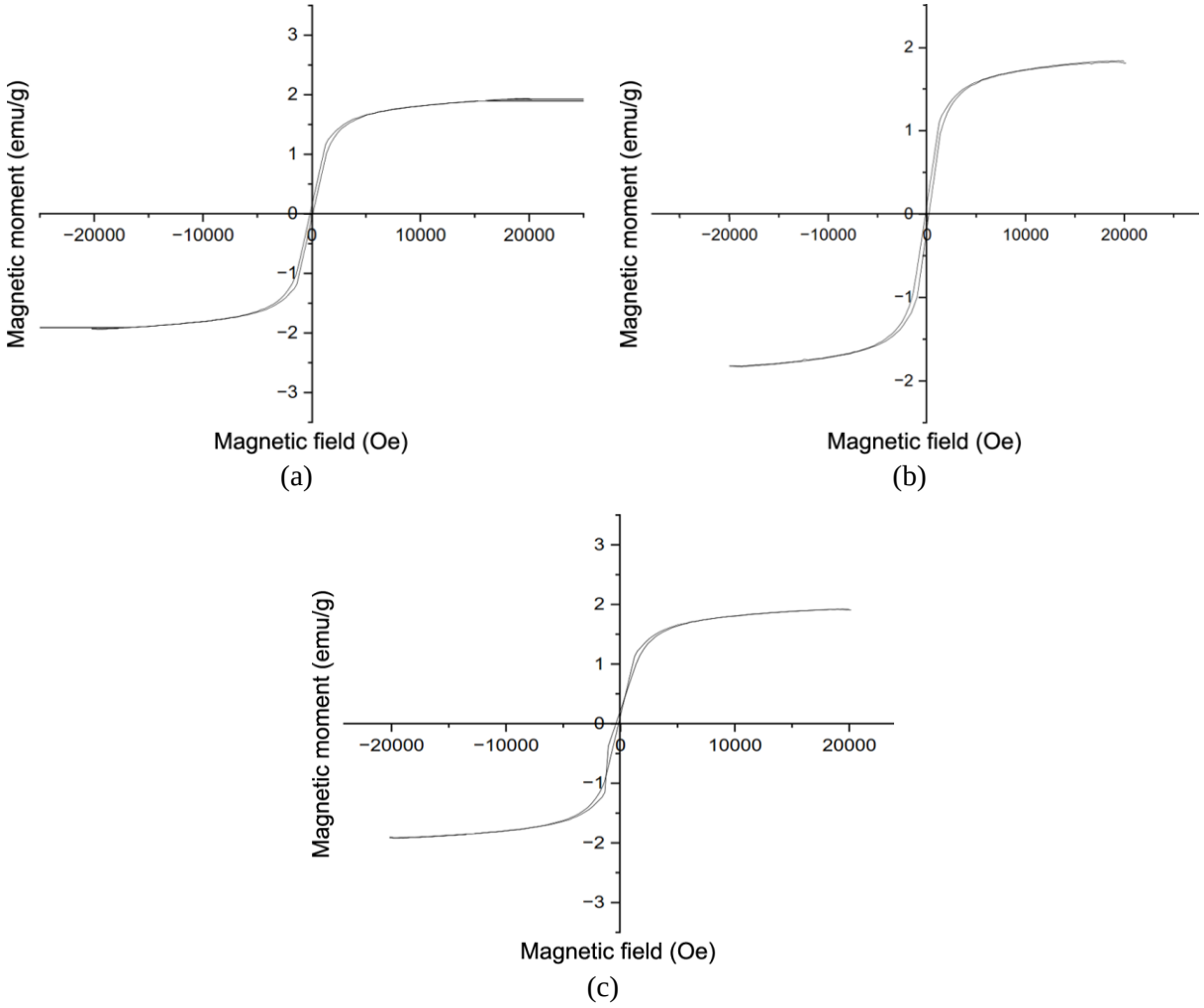

Figure 10. Hysteresis loop curve of the results of the ball milling characterization twith copper doping (a) 0 wt%, (b) 5 wt%, and (c) 10 wt%.

Table 7. Magnetic properties of the VSM characterization test results.

Parameter loop	BM_{2A}	BM_{2B}	BM_{2C}
M_S (emu/g)	1.904	1.817	1.804
M_r (emu/g)	0.1051	0.048	0.1432
H_C (Oe)	126.53	178.39	275.47
Loop squareness	0.055	0.066	0.079
Loop area (kOe.emu/g)	121.9	114.4	128.8

CONCLUSION

The results of this study can be concluded that the magnetic susceptibility value of α-Fe_2O_3 nanoparticles decreased, namely 14441.76×10^{-5}; 14398.76×10^{-5}; and 14364.35×10^{-5} along with the increase in copper doping (wt%) with values in the iron oxide interval. Changes in magnetic properties obtained through VSM are the saturation magnetization value (M_S) which decreased, the coercivity value (H_c) and loop squarness (M_r/M_S) obtained increased with the increase in copper doping given, while the remanent magnetization value (M_r) and the area of the hysteresis loop obtained varied. The results of SEM characterization show the size. The size of the iron oxide particles produced is getting smaller with the increase in copper doping (wt%) given. The copper element increases with the increase in doping concentration (wt%) given, namely 0.76%; 7.11%; and 8.13%. While the Fe element decreased along with the increasing doping concentration given, namely 22.22%; 19.08%; and 18.01%.

REFERENCES

1. Didik, L. A. & Wahyudi, M. (2020). Analisa kandungan Fe dan karakteristik sifat listrik pasir besi Pantai Telindung yang disintesis dengan beberapa metode. *Indonesian Physical Review*, **3**(2), 64–71.
2. Satria, B., Masrurah, Z., & Fajar, S. J. (2021). Magnetic susceptibility and grain size distribution as prospective tools for selective exploration and provenance study of iron sand deposits: A case study from Aceh, Indonesia. *Heliyon*, **7**(12).
3. Nengsih, S. (2018). Potensi nanopartikel magnetit pasir besi Lampanah Aceh Besar melalui studi kajian teknik pengolahan, sintesis dan karakteristik struktur. *CIRCUIT: Jurnal Ilmiah Pendidikan Teknik Elektro*, **2**(1).
4. Yudhawardana, H., & Lalus, H. F. (2023). Analysis of Chemical Compound Content and Magnetic Properties of Iron Sand in Rondo Woing Village, East Manggarai. *Jurnal Pendidikan Fisika Dan Teknologi*, **9**(1), 133–142.
5. Gani, A., Munawar, E., Mamat, R., & Rosdi, S. M. (2023). Investigation of the potential biomass waste source for biocoke production in Indonesia: A review. *Energy Reports*, **10**, 2417s–2438.
6. Royka, A. & Amiruddin, E. (2021). Penentuan nilai suseptibilitas dan ukuran partikel magnetik pasir alam Logas Kabupaten Kuantan Singingi menggunakan variasi ukuran ball milling. *Komunikasi Fisika Indonesia*, **18**(1), 42-47.
7. Widodo, R. D., Anis, S., Ilham, R. I., Firmansyah, H. N., & Wahyuni, N. (2021, March). Shrinkage, Density and Hardness of Hard Magnetic Material (BaFe12O19) Based on Iron Sand Produced by Conventional Solid-State Reaction Process. *IOP Conference Series: Earth and Environmental Science*, **700**(1), 012001.
8. Amiruddin, E., Awaluddin, A., Sihombing, M., Royka, A., & Syahrul, T. (2020). Morphology and structural properties of undoped and cobalt doped magnetic iron oxide particles for improving the environmental quality. *International Journal of Engineering and Advanced Technology (IJEAT)*, **9**(6), 2249–8958.
9. Jia, C., Das, P., Kim, I., Yoon, Y. J., Tay, C. Y., & Lee, J. M. (2022). Applications, treatments, and reuse of plastics from electrical and electronic equipment.

Journal of Industrial and Engineering Chemistry, **110**, 84–99.
10. Cenci, M. P., Scarazzato, T., Munchen, D. D., Dartora, P. C., Veit, H. M., Bernardes, A. M., & Dias, P. R. (2022). Eco-friendly electronics—A comprehensive review. Advanced Materials Technologies, **7**(2), 2001263.
11. Sari, M. N. (2018). *Analisa potensi pemanfaatan limbah pelepah kelapa sawit sebagai bahan dasar elektroda superkapasitor pada industri menengah masyarakat*. Doctoral dissertation, Universitas Islam Negeri Sultan Syarif Kasim Riau.
12. Wei, L. K., Abd Rahim, S. Z., Al Bakri Abdullah, M. M., Yin, A. T. M., Ghazali, M. F., Omar, M. F., Nemeș, O., Sandu, A. V., Vizureanu, P., & Abdellah, A. E. H. (2023). Producing metal powder from machining chips using ball milling process: A review. *Materials*, **16**(13), 4635.
13. Qiram, I. & Rubiono, G. (2021). Pengaruh Penambahan profil pada dinding silinder ball-Mill terhadap distribusi massa serbuk batu bata. *V-MAC (Virtual of Mechanical Engineering Article)*, **6**(2), 52–56.
14. Sitotaw, Y. W., Habtu, N. G., Gebreyohannes, A. Y., Nunes, S. P., & Van Gerven, T. (2023). Ball milling as an important pretreatment technique in lignocellulose biorefineries: A review. *Biomass conversion and biorefinery*, **13**(17), 15593–15616.
15. Bangar, S. P., Singh, A., Ashogbon, A. O., & Bobade, H. (2023). Ball-milling: A sustainable and green approach for starch modification. *International Journal of Biological Macromolecules*, **237**, 124069.